Band-population effects and intraband magneto-optical properties of a many-valley semiconductor: PbTe

H. Burkhard*
Forschungsinstitut der Deutschen Bundespost beim FTZ P.O. Box 5000, D-6100 Darmstadt, Federal Republic of Germany

G. Bauer
Experimentelle Physik IV, Universität Ulm, D-7900 Ulm, Federal Republic of Germany

W. Zawadzki
Institute of Physics, Polish Academy of Sciences, 02-668 Warszawa, Poland
(Received 14 February 1978)

We have performed magnetoreflectivity experiments on n-PbTe epitaxial films using the Faraday configuration ($\vec{B} \| [111]$) in the frequency range of 10–400 cm^{-1} and in magnetic fields up to 14 T. Cyclotron-resonance structures and dielectric anomalies have been observed at frequencies between the TO and LO lattice modes of PbTe. We interpret our results using a free-carrier susceptibility derived within the framework of a linear-response theory. The Landau-level structure has been calculated according to the $\vec{k}\cdot\vec{p}$ approach of Mitchell and Wallis. In the quantitative description of magnetoreflectivity spectra we take into account the magnetic-field-dependent occupation of the Landau states. Fitting our data we determine a set of band parameters for PbTe, which also successfully describe magneto-optical experiments of other authors.

I. INTRODUCTION

A classical description of intraband magneto-optical properties of a narrow-gap semiconductor with the use of an energy-dependent effective mass taken at the Fermi level is often inadequate. For intermediate carrier concentrations several Landau levels are usually occupied within a wide range of magnetic fields.[1] Due to nonparabolicity of the band, magneto-optical transitions originating from different Landau states cannot be described properly with a constant effective mass. In the lead compounds one should, in addition, consider band's anisotropy since the band minima are located at the L point of the Brillouin zone.

In addition, in polar materials the contribution of infrared-active phonons to the total dielectric function is of considerable importance in the frequency range where intraband magneto-optical transitions are usually observed, that is, in the far-infrared region. The lead compounds, in particular PbTe,[2] exhibit a very large TO-LO phonon splitting, the TO mode frequency being temperature dependent, i.e., softens near the center of the Brillouin zone ($\vec{q} \to 0$).

In this paper we obtain information on band parameters from intraband magneto-reflectivity spectra. It turns out that the Wallace model[3] for the multivalley band structure, based on the classical free-carrier oscillator function, is not sufficient to account for the experimentally observed spectra. In order to interpret the data, it is important to consider the variation of the Fermi level as a function of magnetic field. For all directions of the field, except that of $\langle 100 \rangle$, repopulation effects between nonequivalent valleys occur due to different spacings of the Landau ladders.

In the calculation of the Landau levels in PbTe we use the general $\vec{k}\cdot\vec{p}$ treatment of Mitchell and Wallis[4] for the lead compounds. The free-carrier contribution to the total dielectric function is calculated on the basis of a quantum-mechanical formulation (linear-response theory) of the high-frequency magnetoconductivity, taking into account anisotropy and nonparabolicity of the bands involved. We analyze magneto-optical intraband transitions. A discussion of the determined band parameters and their applicability to the description of other experimental data is presented.

In Sec. II we present a short survey of the experiments. The theoretical description is given in Sec. III. Section IV deals with the results and their interpretation. In Sec. V we summarize our conclusions.

II. EXPERIMENTAL

Far-infrared magnetoreflectivity spectra of n-PbTe epitaxial layers were measured in the frequency range of 10–400 cm^{-1}. The samples were grown by the hot-wall technique[5] on $\{111\}$ surfaces of the BaF_2 substrates. They had carrier concentrations between 6×10^{16} and 5×10^{17} cm^{-3} and film thicknesses indicated in Table I. The experiments were performed in

TABLE I. Sample identification.

Sample	Orientation	n (10^{17} cm^{-3})	Thickness (μm)
A 1101	[111]	6.3	19.5
A 83–4	[111]	2.3	14.0
1922	[111]	0.60	15.0
1925–16	[111]	0.80	7.6
2096	[111]	0.97	11.8
2092	[111]	0.80	9.4
A 134–6	[111]	1.67	12.0
1777	[111]	4.8	4.5

Faraday geometry with the magnetic field $\vec{B}\|[111]$ in a gas-flow cryostat at temperatures between 4.2 and 25 K, using Fourier-transform spectroscopy (a Bruker IFS 114 or a Beckman 720 Fourier-transform spectrometer) and Bitter coils or superconducting solenoids. The experimental setup is described in Ref. 6. Frequency dependences of the optical constants of the PbTe films were determined according to the procedure outlined in Ref. 7, taking into account multiple reflections and interference effects in the films and the substrate.

III. THEORY

A. Band model

It is known by now that the lowest conduction band and the highest valence band at the L point of the Brillouin zone of PbTe are not exact mirror images of each other. This is a clear indication, that a two-band model is not sufficient for the calculation of the Landau levels. We use the $\vec{k}\cdot\vec{p}$ approach of Mitchell and Wallis,[4] including exactly the interaction of the lowest conduction ($L_{3^-}^{6^-}$) and the highest valence ($L_{1^+}^{6^+}$) levels of PbTe,[8,9] and incorporating the other four levels ($L_{2^-}^{6^-}$, $L_{3^-}^{45^-}$, $L_{3^+}^{45^+}$, $L_{3^+}^{6^+}$) in k^2 approximation.[4,10,11] The level ordering is taken according to pseudopotential calculations.[8,9] The matrix Hamiltonian describing the $L_{1^+}^{6^+}$ valence and $L_{3^-}^{6^-}$ conduction levels is given by[11]

$$\mathcal{H}=\begin{pmatrix}
\frac{E_g}{2}+\left(\frac{\hbar eB}{m_t^-}\right)(n+\frac{1}{2})+\frac{g_l^-\mu_B B}{2}+\frac{\hbar^2k_B^2}{2m_B^-} & 0 & \left(\frac{E_g}{2m_B}\right)^{1/2}\hbar k_B & [E_g\hbar\tilde{\omega}_{cv}(n+1)]^{1/2}\\
0 & \frac{E_g}{2}+\left(\frac{\hbar eB}{m_t^-}\right)(n+\frac{3}{2})-\frac{g_l^-\mu_B B}{2}+\frac{\hbar^2k_B^2}{2m_B^-} & [E_g\hbar\tilde{\omega}_{cv}(n+1)]^{1/2} & -\left(\frac{E_g}{2m_B}\right)^{1/2}\hbar k_B\\
\left(\frac{E_g}{2m_B}\right)^{1/2}\hbar k_B & [E_g\hbar\tilde{\omega}_{cv}(n+1)]^{1/2} & -\frac{E_g}{2}-\left(\frac{\hbar eB}{m_t^+}\right)(n+\frac{1}{2})-\frac{g_l^+\mu_B B}{2}+\frac{\hbar^2k_B^2}{2m_B^+} & 0\\
[E_g\hbar\tilde{\omega}_{cv}(n+1)]^{1/2} & -\left(\frac{E_g}{2m_B}\right)^{1/2}\hbar k_B & 0 & -\frac{E_g}{2}-\left(\frac{\hbar eB}{m_t^+}\right)(n+\frac{3}{2})+\frac{g_l^+\mu_B B}{2}+\frac{\hbar^2k_B^2}{2m_B^+}
\end{pmatrix}. \tag{1}$$

m_t^+, m_l^+, g_l^+ represent the far-band contributions (in the above sense) to the transverse and longitudinal effective masses and g factors in the valence (+) and conduction (−) bands. $\tilde{m}_{cv}$ is the main contribution to the effective mass coming from the valence-conduction two-band interaction: $\tilde{\omega}_{cv}=eB/\tilde{m}_{cv}$. $m_B^\pm$ are the far-band mass contributions; m_B results from the direct interaction of $L_{1^+}^{6^+}$ and $L_{3^-}^{6^-}$ levels:

$$m_B^\pm = m_t^\pm\cos^2\theta + m_l^\pm\sin^2\theta,$$

$$m_B = \tfrac{1}{2}E_g(\cos^2\theta/P_\parallel^2+\sin^2\theta/P_\perp^2).$$

$P_\parallel$ and $P_\perp$ are interband momentum matrix elements. The 4×4 matrix [Eq. (1)] can be solved exactly for $\vec{B}\|[111]$ in terms of harmonic-oscillator functions, giving the following[11] eigenenergies (for $k_B=0$)

$$\begin{aligned}
E_{v,n,\sigma=+1}^{c,n,\sigma=-1} &= \tfrac{1}{2}(a_n+b_n)\\
&\quad\pm\tfrac{1}{2}[(a_n-b_n)^2+4E_g\hbar\tilde{\omega}_{cv}(n+1)]^{1/2},\\
E_{v,n,\sigma=+1}^{c,n,\sigma=-1} &= \tfrac{1}{2}(c_n+d_n)\\
&\quad\pm\tfrac{1}{2}[(c_n-d_n)^2+4E_g\hbar\tilde{\omega}_{cv}(n+1)]^{1/2},
\end{aligned} \tag{2}$$

where

$$a_n = \tfrac{1}{2}E_g + \hbar\omega_l^-(n+\tfrac{1}{2}) + \tfrac{1}{2}g_l^-\mu_B B\,,$$

$$b_n = -\tfrac{1}{2}E_g + \hbar\omega_l^+(n+\tfrac{3}{2}) - \tfrac{1}{2}g_l^+\mu_B B\,,$$

$$c_n = \tfrac{1}{2}E_g + \hbar\omega_l^-(n+\tfrac{3}{2}) - \tfrac{1}{2}g_l^-\mu_B B\,,$$

$$d_n = -\tfrac{1}{2}E_g + \hbar\omega_l^+(n+\tfrac{1}{2}) + \tfrac{1}{2}g_l^+\mu_B B\,,$$

and

$$\omega_l^{\pm} = eB/m_t^{\pm}\,, \quad \tilde{\omega}_{cv}^{111} = eB/m_{cv}^{111}\,,$$

and

$$m_{cv}^{111}/m_0 = E_g m_0/2P_\perp^2\,.$$

For a magnetic field not parallel to the main ellipsoid axis the matrix Hamiltonian cannot be solved exactly. In this case we use the approximation of Baraff,[12] adapted by Dimmock,[10] solving exactly the two-level model and including the far-band contributions as perturbations. In this approximation the Landau levels are given by Eq. (2) replacing, however, for $g^{\pm} \to \bar{g}^{\pm}$, $\omega^{\pm} \to \bar{\omega}^{\pm}$, and $\tilde{\omega}_{cv} \to \bar{\omega}$:

$$\bar{g}^{\pm} = \frac{P_\parallel g_t^{\pm}\sin^2\theta + P_\perp g_l^{\pm}\cos^2\theta}{(P_\parallel^2\sin^2\theta + P_\perp^2\cos^2\theta)^{1/2}}\,,$$

$$\bar{\omega}^{\pm} = \frac{\tfrac{1}{2}(P_\parallel^2\omega_l^{\pm 2} + P_\perp^2\omega_t^{\pm 2})\sin^2\theta + P_\perp^2\omega_l^{\pm 2}\cos^2\theta}{\omega_l^{\pm}P_\perp(P_\parallel^2\sin^2\theta + P_\perp^2\cos^2\theta)^{1/2}}\,,$$

where $\omega_t^{\pm} = eB/(m_t^{\pm}m_l^{\pm})^{1/2}$ and

$$\bar{\tilde{\omega}}_{cv} = (2eB/E_g m_0^2)P_\perp(P_\parallel^2\sin^2\theta + P_\perp^2\cos^2\theta)^{1/2}\,.$$

For $k_B \neq 0$ it is not possible to give simple exact expressions for the energies even for $\vec{B}\|[111]$. We observe, however, that, if one neglects far-band contributions the exact solutions can be found, having a term $E_g\hbar^2k_B^2/2m_B$ under the square root. It is then a good approximation in our range of energies to include the k_B dependence by inserting the above term under the square roots of Eq. (2), which corresponds to exact solutions at $k_B = 0$ and two-band solutions for the k_B dependence. For example, the error in energy, as compared to the numerical diagonalization of Eq. (1) is less than 5% for $n \leq 5\times10^{17}$ cm^{-3} and $B = 3$ T. It should be mentioned that the valence and the conduction bands are both nonparabolic and nonspheroidal. We are not concerned here with problems arising from the nonspheroidal nature of the Fermi surface in PbTe. A detailed discussion of this problem was given by Adler *et al.*[13]

According to Eq. (2) the highest valence and the lowest conduction Landau levels are $E_{v,-1,\sigma=-1} = b_{-1}$ and $E_{c,-1,\sigma=-1} = c_{-1}$. In the following we use a more physical notation for the Landau levels (cf. Ref. 11) by raising the n numbers of the $|-\rangle$ states by one and assigning an effective spin of $\pm\frac{1}{2}$ to the $|\pm\rangle$ states.

B. Fermi energy

For the interpretation of intraband magneto-optical data it is important to know the number of carriers in different valleys.

The electron occupation of the different valleys depends on the orientation as well as on the magnitude of the applied magnetic field. This redistribution between valleys nonequivalent with respect to the magnetic field, as compared to the no-field case, is brought about by the Landau quantization. For the possible magneto-optical transitions in an equivalent set of valleys the energetic position of the Fermi level with respect to the bottom of the lowest Landau level is of importance. Using the condition that the total number of free carriers N is a constant, the variation of Fermi energy with magnetic field can be calculated numerically from the following relation:

$$N = \frac{1}{4\pi^2}\frac{eB}{\hbar}\sum_s\sum_{n,\sigma}\int_{-\infty}^{\infty} f(E_{n,k_B,\sigma}, E_F, T)\,dk_B\,, \tag{3}$$

where E_F denotes the Fermi energy, $\hbar k_B$ is the momentum in the direction of the magnetic field, and f is the Fermi-Dirac distribution function. The summation extends over the number of valleys s ($s = 4$ for PbTe). We have calculated the variation of the Fermi energy with magnetic field for $\vec{B}\|[111]$ using Eq. (3). Figure 1 shows the $E_F(B)$ dependence for the electron concentration of

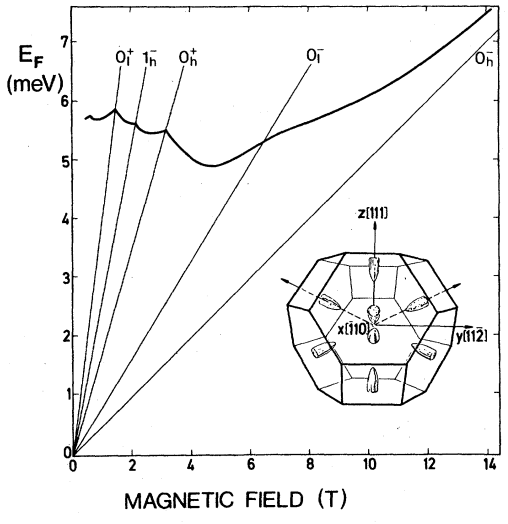

FIG. 1. Variation of the Fermi energy with magnetic-field intensity for the PbTe sample 1925-16, $\vec{B}\|[111]$. The numbers denote Landau-level numbers where $n_{\hbar}^{\pm}$ denote $n|\pm\rangle$ states for the levels associated with the $\langle 111\rangle$ valleys and $n_l^{\pm}$ the levels associated with the [111] valley.

$N = 8 \times 10^{16}$ cm^{-3}. It can be seen that for the magnetic fields below 7 T more than one Landau level is populated.

C. Dielectric function

1. Classical model

In the Faraday configuration ($\vec{B} \| \vec{q}$) the dielectric function for the two circularly polarized modes ($\pm$) is given by a sum of several susceptibility contributions[14]:

$$\epsilon^{\pm} = 1 + \chi \text{ (valence electrons)} + \chi \text{ (polar phonon)} + \chi^{\pm} \text{ (free carriers)}. \quad (1)$$

For the free-carrier contribution a classical oscillator model, taking into account ellipsoidal surfaces of constant energy, was developed by Wallace.[3] For both p- and n-type PbTe with $\vec{B} \| [111]$, two cyclotron-resonance frequencies ω_{c1} and ω_{c2} appear: one determined by the transverse effective mass m_T (resonance of the carriers in the ellipsoid with its long axis oriented along [111]), and one determined by $m_{c2} = 3m_T[m_L/(8m_T + m_L)]^{1/2}$ (resonance in the three ellipsoids with their long axis parallel to one of the $\langle \bar{1}11 \rangle$ directions). This model was used by Buss and Kinch[15] for fitting intraband magnetoreflectivity data of PbTe bulk samples in the far infrared. Burkhard *et al.*[6] and Ramage *et al.*[16] also used this model to describe both magnetoreflectivity and magnetotransmission data taken on epitaxial n- and p-PbTe samples.

For the orientation $\vec{B} \| [111]$ the electronic contribution to the susceptibility is given by

$$\chi^{\pm} \text{ (free carriers)} = -\frac{\omega_p^2 (m_0/m_T)(\omega \mp \omega_{c1} - i\omega_{\tau_1})}{4\omega[(\omega \mp \omega_{c1})^2 + \omega_{\tau_1}^2]} - \frac{\omega_p^2[a(\omega + i\omega_{\tau_2}) \pm b\omega_{c1}](\omega^2 - \omega_{c2}^2 - \omega_{\tau_2}^2 - 2i\omega\omega_{\tau_2})}{\omega[(\omega^2 - \omega_{c2}^2 - \omega_{\tau_2}^2)^2 + 4\omega^2\omega_{\tau_2}^2]}, \quad (4)$$

where

$$\omega_p^2 = ne^2/\epsilon_0 m_0, \quad \omega_{c1} = eB/m_T,$$
$$\omega_{c2} = [(1/9m_T)(8/m_L + 1/m_T)]^{1/2} eB,$$
$$a = \tfrac{1}{12} m_0 (4/m_L + 5/m_T),$$
$$b = \tfrac{1}{12} m_0 (8/m_L + 1/m_T);$$

$\omega_{\tau_1}, \omega_{\tau_2}$ are the damping parameters for the carriers in the [111] and $\langle \bar{1}11 \rangle$, the three oblique valleys, with respect to $\vec{B} \| [111]$.

Equation (4) implies that one-fourth of the total number of carriers occupies the [111] valley ($\frac{1}{4}\omega_p^2$) and the remaining three-fourths occupy the other three equivalent $\langle \bar{1}11 \rangle$ valleys. Since the valley populations are determined by the variation of the two [111] and $\langle \bar{1}11 \rangle$ Landau ladders one must adopt a valley repopulation approach in order to use the Wallace model. As far as the damping problems are concerned the damping parameter of one resonance can influence the other resonance. In the interpretation of experimental results some authors use two different damping parameters for the resonances. In Fig. 2 the real and imaginary parts of the total dielectric function are plotted using Eq. (4) for the electronic contribution. A classical oscillator model was used to describe polar phonon contribution.

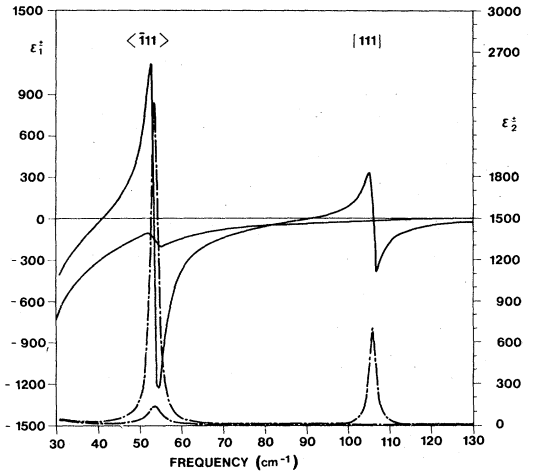

FIG. 2. Real ($\epsilon_1^{\pm}$: solid line) and imaginary part ($\epsilon_2^{\pm}$: dot-dashed line) of the dielectric function, calculated according to the Wallace model [Eq. (4)], as a function of frequency for:

$n = 8 \times 10^{16}$ cm^{-3} $\omega_{\tau 1} = \omega_{\tau 2} = 1.0$ cm^{-1},
$m_T/m_0 = 0.0235$, $m_L/m_0 = 0.15$, $B = 2.78$ T ($\vec{B} \| [111]$),
$\omega_{TO} = 17.5$ cm^{-1}, $\omega_{LO} = 114$ cm^{-1}, $\epsilon_s = 1350$.

However, the validity of this model is limited if applied to PbTe, due to the following shortcomings.

(a) Magnetic field dependence of the cyclotron masses should be introduced to account for band nonparabolicity. In an intermediate magnetic field range, when several Landau levels are occupied, inter-Landau level transitions cannot be characterized by a single cyclotron mass.

(b) If nonparabolicity is taken into account properly, the line shape of the spectra will deviate from that given by a Lorentzian distribution. Due to band nonparabolicity the transition energies depend on k_B, the highest corresponding to $k_B = 0$. This leads to an increase of the imaginary part ϵ_2 for frequencies lower than the transition

frequency at $k_B = 0$, as compared to the classical model. This fact modifies ϵ_1 as well.

2. Linear-response theory

To circumvent these problems and to take into account the actual band structure properly, the free-carrier contribution to the dielectric function was calculated using a linear-response theory for the high-frequency conductivity in a quantizing magnetic field:

$$\chi^{\pm}\ (\text{free electrons}) = \frac{i}{\epsilon_0 \omega} \sum_s \sigma_s^{\pm}, \tag{5}$$

where $\sigma_s^{\pm}$ is the high-frequency conductivity due to valley s for "right" and "left" ($\pm$) circular polarization. In the long-wave length limit it is given by[17,18]

$$\sigma_s^{\pm}(\omega, \vec{q} \to 0) = i \frac{e^2 N_s}{m_0 \omega} \{\alpha_T - \tfrac{1}{2}(\alpha_T - \alpha_L)\sin^2\theta_s\} + \frac{i}{\hbar\omega} \sum_{n,n',\sigma} \sum_{k_y,k_B} \frac{M_{\pm}^2[f(E_{n,k_B,\sigma,s}) - f(E_{n',k_B,\sigma,s})]}{(1/\hbar)(E_{n',k_B,\sigma,s} - E_{n,k_B,\sigma,s}) - \omega - i\xi}, \tag{6}$$

where θ_s is the angle between B and the orientation of the long axis of valley s. We set $\alpha_T = m_0/m_T$, $\alpha_L = m_0/m_L$, while f is the Fermi-distribution function. n and n' are Landau-level quantum numbers and σ denotes the spin quantum number; ξ is the damping parameter and E is Landau-level energy. The transition-matrix elements are given by[18]

$$\begin{aligned} M_+^2 &= (e^2/m_0)[\gamma_s'^2(n'+1)\delta_{n',n-1} + \gamma_s^2 n' \delta_{n',n+1}] \\ &\quad \times (E_{n',k_B,\sigma,s} - E_{n,k_B,\sigma,s}), \\ M_-^2 &= (e^2/m_0)[\gamma_s^2(n'+1)\delta_{n',n-1} + \gamma_s'^2 n' \delta_{n',n+1}] \\ &\quad \times (E_{n',k_B,\sigma,s} - E_{n,k_B,\sigma,s}), \end{aligned} \tag{7}$$

where

$$\gamma_s = \tfrac{1}{2}(\sqrt{\alpha_T} + \sqrt{\zeta_s}), \quad \gamma_s' = \tfrac{1}{2}(\sqrt{\alpha_T} - \sqrt{\zeta_s}),$$

with

$$\zeta_s = \alpha_T - (\alpha_T - \alpha_L)\sin^2\theta_s .$$

The summation $\sum_{k_y,k_B}$ is replaced by $(eB/4\pi^2\hbar)\int_{-\infty}^{\infty} dk_B$. N_s denotes the carrier concentration in valley s and it depends on magnetic field B through the position of the Fermi level E_F. Taking into account band's nonparabolicity, the magnetic-field-independent contribution to $\sigma_s^{\pm}(\omega)$ in Eq. (6) (first term) has to be averaged over energy according to Zawadzki,[19] with the curly brackets meaning an integral average according to the procedure outlined in Eqs. (5) and (254) of Ref. 19.

Whereas for the calculation of the transition energies and the occupation probabilities we used the expressions presented in Sec. III A, for the intraband matrix elements we neglected the k_B dependence of the intraband matrix elements and used a parabolic approximation for $M_{\pm}^2$. The problems associated with the introduction of the broadening factor ξ to expressions like Eq. (6) are common to all treatments of $\sigma(\omega, B)$, and they were discussed by Tosima *et al.*[20]

As in the classical oscillator model, for the three ellipsoids with long axis inclined with respect to B the eigenmodes are no longer circular but elliptical. Thus, there does not exist a pure active or inactive mode and the carriers in these three valleys will exhibit a resonance behavior also for the inactive sense of circular polarization of the incoming electromagnetic wave.[14]

The variation of the Fermi energy E_F as a function of magnetic field intensity for a fixed field direction and carrier concentration is obtained numerically from Eq. (3), which allows us to determine the population of the four $\langle 111 \rangle$ valleys. This information enables us to use Eqs. (5)–(7) to calculate the free-carrier susceptibility contribution to the total dielectric function.

In Fig. 3 we have plotted the real (ϵ_1) and imaginary part (ϵ_2) of the total dielectric function for a magnetic field of 2.78 T ($\vec{B} \| [111]$), with the free-carrier contribution calculated according to the procedure outlined above. Also included are data on the free-carrier susceptibility contributions to ϵ_1 and ϵ_2 separately. These curves deviate considerably from those calculated with the classical oscillator model,[3] especially in their asymmetries with respect to the resonance frequencies (see Fig. 2).

IV. RESULTS AND ANALYSIS

A. Lattice parameters

Apart from all the problems associated with the band structure and the proper free-carrier contribution to the dielectric function, one needs to know the lattice parameters determining the optical properties of the films and substrate.

Reflectivity spectra of all samples were taken also at $B = 0$ and the phonon parameters of the PbTe films: ω_{TO}, ω_{LO}, ϵ_s, and ϵ_∞ and Γ were

determined. This is described in detail in Refs. 7 and 21. The classical oscillator model is used for the polar phonon contribution to the dielectric function:

$$\chi\ (\text{polar phonon}) = \frac{\omega_{TO}^2(\epsilon_s - \epsilon_\infty)}{\omega^2 - \omega_{TO}^2 - i\omega\Gamma},$$

where ϵ_s is the static and ϵ_∞ is the high-frequency dielectric constant, while Γ is the damping parameter. ω_{TO} and corresponding ϵ_s were found to depend not only on temperature but also on the carrier and total vacancy concentration.[21] For our epitaxial films the frequency ω_{TO} (PbTe) varied between 17.5 ± 0.5 and 18.5 ± 0.5 cm^{-1} at helium temperature, increasing with increasing carrier concentration. This behavior is consistent with a model for TO phonon mode softening, based on electron–TO-phonon interband interaction, as proposed by Kawamura *et al.*[22] For ω_{LO} a value of 114 cm^{-1} resulted and Γ varied from 0.2 to 1.5 cm^{-1}. ϵ_s ranges from 1300 to 1650. Multiparameter descriptions of reflectivity spectra of Pb-compound epitaxial layers were also carried out by Tennant and Cape[23] and Amirtharaj *et al.*[24]

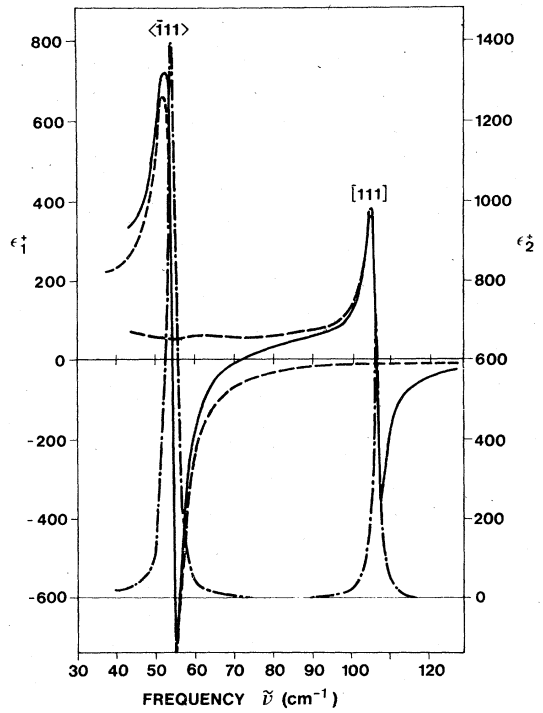

FIG. 3. Real (ϵ_1: solid and dashed lines) and imaginary part (ϵ_2: dot-dashed line) of the dielectric function, calculated using $\vec{k}\cdot\vec{p}$ model according to Eq. (3), as a function of frequency for : $T = 10$ K, $E_F = 5.7$ meV, $E_g = 190$ meV, $\xi = 1$ cm^{-1}, $\omega_{TO} = 17.5$ cm^{-1}, $\omega_{LO} = 114$ cm^{-1}, $\epsilon_S = 1350$ for $B = 1.78$ T, $\vec{B} \parallel [111]$.

B. Magnetoreflectivity spectra

Typical magnetoreflectivity spectra are shown in Figs. 4(a) and 4(b). The dips are associated with cyclotron resonance in the [111] and ⟨1̄11⟩ valleys, respectively. The minimum at the lowest frequency for a given magnetic field is due to a dielectric anomaly (zero of the dielectric function). Additional dips are associated with interference effects in the Fabry-Perot-like PbTe films. With increasing magnetic field the magnetoreflectivity dips shift towards higher frequencies. The coupled plasmon-phonon frequency $\omega_{LO}^+ = (\omega_p^2/\epsilon_\infty + \omega_{LO}^2)^{1/2}$ (for $B = 0$, neglecting damping) is higher than the cyclotron-resonance frequencies, making the sample opaque and almost totally reflecting for magnetic fields at which $\omega > \omega_c$. A multiparameter fit has been performed using Wallace model[3] and the results are shown in Figs. 4(a) and 4(b). The cyclotron-resonance frequencies are fairly well described. The details of the structures below the resonance, however, are not represented satisfactorily.

Another shortcoming of the simple classical model is demonstrated in Fig. 5, where the two cyclotron frequencies determined from fits to magnetoreflectivity data as a function of frequency for various magnetic fields are presented. Samples having different carrier concentrations yield different slopes of the ω_{c1} and ω_{c2} curves as functions of magnetic field. The frequencies ω_{c1} and ω_{c2} represent averages over transition energies, and thus it is hardly possible to deduce directly band-edge masses and band nonparabolicity from these data.

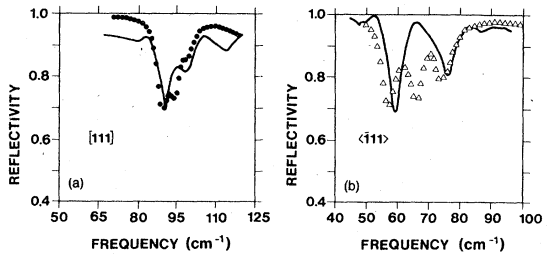

FIG. 4. (a) (Left part) magnetoreflectivity vs frequency for sample 1925-16 at $B = 2.48$ T (resonance associated with carriers in the [111] valley, $\vec{B} \parallel [111]$); solid line experimental data; (●) calculation according to the Wallace model (Eq. 4). Parameters: $n = 8 \times 10^{16}$ cm^{-3}, $\omega_\tau = 1.5$ cm^{-1}, $m_T/m_0 = 0.0235$, $m_L/m_0 = 0.15$, $B = 2.48$ T ($\vec{B} \parallel [111]$); $\omega_{TO} = 17.5$ cm^{-1}, $\omega_{LO} = 114$ cm^{-1}, $\epsilon_S = 1350$; (b) as (a), resonance structures as associated with carriers in the three ⟨1̄11⟩ valleys. Solid line, experimental data; Δ, calculation. Parameters: $B = 4.11$ T, $m_T/m_0 = 0.0245$, $m_L/m_0 = 0.155$, $\omega_\tau = 1.5$ cm^{-1}. In general, the classical-model fit does not describe details of the structures below cyclotron resonance satisfactorily.

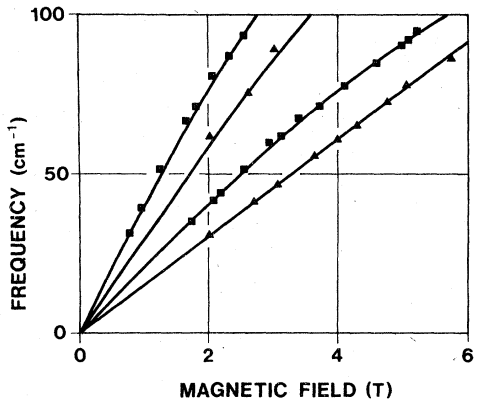

FIG. 5. Cyclotron-resonance frequencies ω_{c1} ($\propto 1/m_T$) and ω_{c2} [$\propto [(1/9m_T)(8/m_L + 1/m_T)]^{1/2}$] as determined from magnetoreflectivity spectra using a classical model dielectric function parameter fit as shown in Figs. 4(a) and 4(b): experimental data for sample PbTe 1922 (■), ($n = 6.0 \times 10^{16}$ cm^{-3}) and PbTe A 1101 (▲), ($n = 6.3 \times 10^{17}$ cm^{-3}). Apparent resonance frequencies determined from the classical model decrease with increasing carrier concentration.

Using a dielectric function calculated according to Eqs. (5)–(7) a better agreement with the experimental data can be obtained. This is shown in Figs. 6(a) and 6(b), where the same data as in Figs. 4(a) and 4(b) are compared with the calculation. The comparison has been carried out in the following way: Having determined the lattice contribution to the dielectric function one obtains the exact position of the Fermi level and its variation with magnetic field. For the sample of Figs. 6(a) and 6(b) the Fermi energy vs B, as determined from Eq. (3), is shown in Fig. 1. Next, using the dielectric function according to Eqs. (5)–(7) a fit, as indicated in Figs. 6(a), and 6(b), is obtained. For the resonances associated with the carriers in the $\langle \bar{1}11 \rangle$ and [111] valleys we use a k_B-independent electron damping parameter ξ. Depending on the lattice temperature, we used values for ξ ranging from 0.8 to 1.5 cm^{-1}.

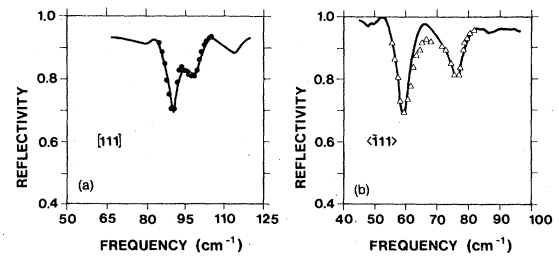

FIG. 6. (a) (Left part) magnetoreflectivity vs frequency for sample PbTe 1925-16 at $B = 2.48$ T and T = 15 K (resonance associated with carriers in the [111] valley, $\vec{B} \parallel [111]$), (solid line) experimental data; ● calculation as described in the text is based on linear response expression for $\chi^{\pm}$. (b) As above, resonance structures associated with carriers in the three $\langle \bar{1}11 \rangle$ valleys. $B = 4.11$ T. (Solid line) experimental data; Δ calculation.

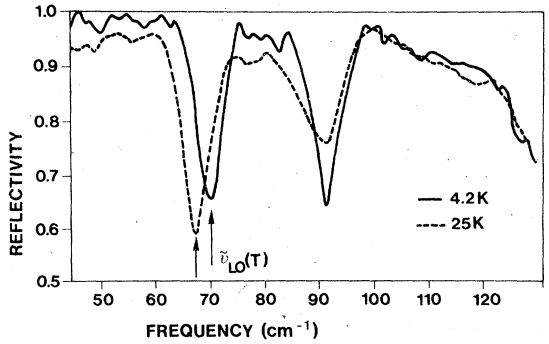

FIG. 7. Magnetoreflectivity spectra of sample 1925-16 for $B = 5.15$ T vs frequency at two different lattice temperatures. The lower dip is due to a dielectric anomaly ($\tilde{\nu}_{LO}$), the higher one is associated with the resonance in the $\langle \bar{1}11 \rangle$ valleys. The resonance due to electrons in the [111] valley is no longer resolvable. With increasing temperature broadening, a frequency shift of the resonant structures occurs.

C. Temperature dependence of the magnetoreflectivity spectra

The experimentally observed magnetoreflectivity spectra exhibited a considerable dependence on temperature. An example is shown in Fig. 7. The resonant structures shift due to the temperature dependence of the cyclotron transition frequencies and the associated dielectric anomalies. In addition, this shift is also influenced by the thermal excitation of carriers if band nonparabolicity is taken into account. The position of the arrows indicates the lowest dielectric anomaly $\tilde{\nu}_{LO}$. The dielectric anomalies are determined by the condition $\mathrm{Im}[-\omega/\hat{\epsilon}(\omega)] = \max$. For negligible damping this can be approximated by $\mathrm{Re}\hat{\epsilon} = 0$, which we have used.

The measurements at different temperatures were performed at various magnetic fields. Figure 8 shows the frequency difference of the sharp-

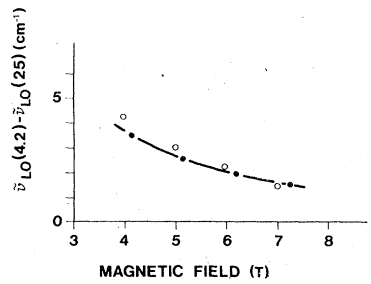

FIG. 8. Difference of dielectric anomaly dips $\tilde{\nu}_{LO}$ (4.2 K) − $\tilde{\nu}_{LO}$ (25 K) vs magnetic field. ●: measured values; O: calculated values, as described in the text.

est structures, the lowest dielectric anomaly dips $\tilde{\nu}_{LO}$ (sharp minima in reflectivity) for two different temperatures as a function of B. Together with these experimental data, the position of the calculated difference frequencies $\tilde{\nu}_{LO}(25\ K) - \tilde{\nu}_{LO}(4.2\ K)$ are shown. The total dielectric function obtained from the linear response expressions $\chi^{\pm}$ was used in the calculation. The shift of the dielectric anomaly to lower frequencies with increasing temperature is mainly due to two reasons:

(a) Increasing energy gap results in the increase of the band-edge mass.

(b) Electrons are thermally excited to higher Landau levels. As a consequence, ϵ_1 and ϵ_2 increase at lower frequencies and the zero of the real part of the total dielectric function shifts into this direction.

This comparison is another test for the applicability of our model calculations which explain the shift of the resonances with temperature.

D. Pinning phenomena

The cyclotron frequencies in our experiments occur in a frequency range between the TO and LO lattice mode frequencies. For sufficiently high magnetic fields, the cyclotron frequencies approach LO mode frequencies.

A pinning of the observed cyclotron resonance structures is found at frequencies higher than the bare LO phonon frequency.[6,25] This resonant interaction differs from the one observed in relatively pure semiconductors, when ω_c approaches ω_{LO}, due to the high carrier concentration of our samples, and thus due to the fact that in this case carrier-carrier interactions might be not negligible.[26]

The above pinning phenomena can be explained neither on the basis of classical magnetopolar-phonon-plasmon modes in the Faraday configuration[14,15,27] nor by plasmon-electron interaction described in Ref. 28. Recently, Ramage *et al.*[16] have reported a similar pinning in p-PbTe.

Resonant magnetopolaron effects in semiconductors with high carrier concentrations were recently studied by Vogl.[18] It has been shown that strong pinning phenomena can occur by a hybridization of many-particle states which involve single as well as collective excitations and phonons. A theoretical and numerical analysis carried out in Refs. 18 and 29 yielded a pinning of singularities of the electronic susceptibility towards $\omega_{LO} + E_F^0(B)/\hbar$, where E_F^0 is the Fermi energy counted from the 0^- level ($E_F = E_{c,0,-1} + E_F^0$). The experimentally observed pinning of the cyclotron-resonance structure is in qualitative agreement with this result. Because of the decrease of $E_F^0(B)$ with increasing B, the frequency ω_{c1} pins to a higher frequency than ω_{c2}, which approaches $\omega_{LO} + E_F^0$ at higher fields. This pinning frequency depends on carrier concentration, increasing with increasing n, as observed experimentally in Refs. 6, 25, and 16.

The pinning phenomena also have consequences for the dielectric anomalies. This is demonstrated in Fig. 9 for the dielectric anomaly lying below ω_{c2}. The dots represent the corresponding reflectivity minima and the dashed curve is a calculation based on the band model of Sec. III, using the variation of $E_F(B)$ also shown in this figure. This dashed curve is obtained from $\mathrm{Re}(\hat{\epsilon}) = 0$ using Eqs. (5)–(7) for the electronic contribution to the total dielectric function.

Also as a consequence of the pinning phenomena the dielectric anomaly exhibits a considerable decrease of the slope of $\tilde{\nu}_{LO}$ versus magnetic field at high fields (see dots in Fig. 9). A consistent calculation of these deviations based on the correct band model and on the resonant magnetopolaron effects is beyond the scope of this work.

E. Band parameters

We measured a large number of reflectivity curves at various magnetic fields. These spectra were fitted by the procedure outlined in Secs. III A–III C. Even a rough analysis (see, e.g., Fig. 4) shows that a simple two-band model is not appropriate to account for the data. The L_3^{6-} conduction band is less nonparabolic than predicted by the two-band model, which is related to the far-band contributions. In addition,

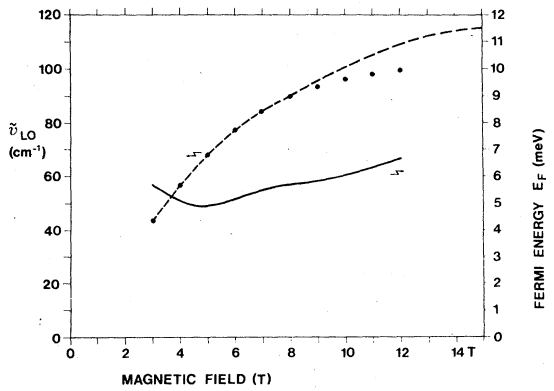

FIG. 9. Dielectric anomaly $\tilde{\nu}_{LO}$ and Fermi energy vs magnetic field. ● represent experimental values (sample number: PbTe 1925-16). The calculated values of $\tilde{\nu}_{LO}$ (dashed line) taking into account the variation of the Fermi energy E_F with B agree up to 8 T with experiments, above 8 T (dashed line) a deviation occurs due to resonant magnetopolaron interaction.

intravalence band magnetotransmission experiments[16] have shown that the band-edge masses in the valence band are different from those of the conduction band. A two-band model would imply exact mirror images (apart from a small free-electron term).

As our intraband magnetoreflectivity measurements are not sufficient to determine all parameters of the $\vec{k}\cdot\vec{p}$ model presented in Sec. III A, we had to rely on other measurements: (a) Conduction-band spin-flip data[30]; (b) cyclotron resonance in the L_{1+}^{6+} valence band[16]; (c) interband transitions[31,32]; (d) cyclotron resonance harmonics[11]; (e) pseudopotential energies[8]; and (f) temperature dependence of band gap E_g.[33] In addition, the related data from magnetotransport measurements, as compiled by Hewes *et al.*,[34] imposed a constraint on the possible set of band parameters. It should be noted that, in principle, even a set of band parameters explaining consistently all available magneto-optical data is not necessarily unique. Small variations of the two-band matrix elements can be counterbalanced by corresponding adjustments of the far-band parameters.

The starting point of the fit program for our magneto-optical data was a set of $\vec{k}\cdot\vec{p}$ parameters which described the measurements (a)–(d) These parameters were next altered in successive steps to provide a good description of our data. The changes of the parameters were made in such a way that the constraints (a)–(f) were satisfied.

Since the intraband transition energies are determined by the direct interaction of the L_{3-}^{6-} and L_{1+}^{6+} levels and by the far-band interactions a separation of the two is not possible. However, certain interband magneto-optical data allow a determination of only far-band interactions. The magnetic field dependence of the lowest conduction level ($E_{c,0,-}$) and the highest valence level ($E_{v,0,-}$) is governed by the far bands alone. Interband transitions between these levels have been observed by several workers.[32] These measurements were used as an additional check on our far-band parameters. The intraband transition energies of the carriers in the [111] valley do not depend on the longitudinal-direct-interband-momentum matrix element $P_{\|}$. This is of additional aid in the determination of $P_{\perp}$. The lowest magnetic field to which the optimum values of $P_{\|}$ and $P_{\perp}$ are applicable is 1 T.

The set of band parameters obtained that way are given in Table II. The band parameters are presented in Mitchell-Wallis sign convention, together with the pseudopotential level energies.[8]

In PbTe there is a considerable variation of the direct energy gap E_g with temperature. For a fit of the reflectivity spectra taken at different temperatures we used the variation of $E_g(T)$ as determined by Antcliffe and Parker.[33] We neglected variations of the far-band contributions with temperature, since to our knowledge no precise experimental data are available for the distant gaps.

As shown in Secs. III A–III C, the lattice parameters of the PbTe film enter into the dielectric function and thus influence positions of the magnetic-field-induced singularities and anomalies. It is therefore important to determine how much the lattice parameters can affect the $\vec{k}\cdot\vec{p}$ parameters. For example, for a carrier concentration of 8×10^{16} cm^{-3} a change of ω_{TO} from 17.5 to 10 cm^{-1} and a corresponding increase of ϵ_s shifts a singularity at 60 cm^{-1} (3 T) by less than 1 cm^{-1} downwards. For the singularity at 40 cm^{-1} the corresponding shift would be less than 1.5 cm^{-1}. However, if the frequencies were further reduced into the neighborhood of ω_{TO}, substantial errors would be unavoidable without exact knowledge of the lattice parameters.

For the determination of the band parameters from magneto-optical data it is necessary to take the resonant magnetopolaron effects into account by restricting the range of magnetic fields at which reflectivity spectra were used for the fitting procedures. Otherwise considerable errors in-

TABLE II. Pseudopotential level energies and parameters at the L point.

$E_g = L_{3-}^{6-} - L_{1+}^{6+} = 0.1895$ eV [a]	$L_{3-}^{6-} - L_{3+}^{45+} = 0.979$ eV [b]	$L_{2-}^{6-} - L_{1+}^{6+} = 1.33$ eV [b]
	$L_{3-}^{6-} - L_{3+}^{6+} = 1.523$ eV [b]	$L_{3-}^{45-} - L_{1+}^{6+} = 1.278$ eV [b]
$2P_{\perp}^2/m_0 = 5.9 \pm 0.2$ eV	$m_l^+/m_0 = -0.095 \pm 0.01$	$g_l^+ = +1 \pm 0.2$
	$m_l^-/m_0 = +0.07 \pm 0.007$	$g_l^- = -3 \pm 0.6$
$(P_{\perp}/P_{\|})^2 = 10.24 \pm 0.6$	$m_l^+/m_t^+ = 7.84 \pm 2$	$g_t^+ = 0.36 \pm 0.08$
	$m_l^-/m_t^- = 5.9 \pm 2$	$g_t^- = -1.5 \pm 0.3$

[a] For $T = 0$ K.
[b] Reference 14.

dicating a too strong nonparabolicity of the band would result.

V. DISCUSSION AND CONCLUSIONS

The interpretation of far infrared magneto-reflectivity spectra of n-PbTe was performed, based on a $\vec{k}\cdot\vec{p}$ model for the valence and conduction bands and a linear response theory for the electron susceptibility. A quantitative description of the reflectivity structure was possible.

Since even the purest PbTe material available until now is still degenerate, the position of the Fermi level and its variation with B is decisive for the shape of the magnetoreflectivity spectra. Thus, quantitative data can only be obtained by taking properly into account the band-population effects in the presence of a magnetic field. For this reason even in the purest available samples no exact data on the cyclotron-resonance frequencies can be directly derived from the reflectivity structure. In addition, experiments in a frequency range $\omega_{TO} < \omega_c < \omega_{LO}$ can be properly explained only if the polar phonon contribution to the total dielectric function is taken into account.

Despite a large amount of work on PbTe, the dispersion of the reported values for the lattice parameters ϵ_s and ω_{TO} as well as the band parameters is still large.[35] Bauer *et al.*[21] and Kawamura *et al.*[36] have shown recently that ϵ_s and ω_{TO} depend on the carrier concentration and on the total concentration of lattice defects, which explains at least some of the discrepancies.

Intraband magneto-optical transitions induced by far-infrared radiation usually provide an effective technique for determining band parameters. In PbTe, for frequencies between 20 and 100 cm^{-1}, $\omega\tau$ approaches 100 and more, so that sharp resonant structures can be expected. However, the difficulties with the lattice contributions to the dielectric function and with the band-population effects substantially complicate the analysis of the experimental data. Some recent reports on magneto-optical intraband data yield quite different band parameters, especially as far as the band-edge effective masses are concerned. Drew and McKnight,[37] and Foley and Langenberg[35] reported band-edge mass values which are about 20% to 30% smaller than often quoted numbers. Foley and Langenberg[35] used microwave frequencies, having necessarily somewhat poorer resolution than that obtainable with far-infrared techniques and encountering problems arising from nonlocal effects. However, the discrepancy of these results is so large, that they are most probably not due to experimental uncertainties. The results of Foley and Langenberg[35] yield also the smallest values of ω_{TO} and the highest ones of ϵ_s reported so far. There exist observations[36] suggesting that the "static" dielectric constant values determined from far infrared and microwave techniques are different, indicating that there must be some additional oscillators below the ω_{TO} frequency. Based on a recent suggestion by Burns and Burstein[38] we have shown that local modes associated with the vacancies may be responsible for a further increase of "ϵ_s" with decreasing frequency.[21] If these local modes exist, then the microwave results of Foley and Langenberg could be possibly influenced by these effects.

Our magnetoreflectivity spectra are not influenced by surface-space-charge effects. Schaber *et al.*[39] found that in as-grown epitaxial PbTe samples of the same source, a flat-band condition prevails.

The band parameters we determined describe our magnetoreflectivity data, the conduction-band g factors, the cyclotron resonance in the valence band, and the magneto-optical interband reflection data (cf. Ref. 17). This provides the necessary test for the validity of the band model and the obtained values.

VI. ACKNOWLEDGMENTS

We are indebted to Professor K. Dransfeld and Professor P. Grosse for their interest and support of this work. We thank Dr. P. Vogl for helpful discussions on the linear-response formulation for the dielectric function. The samples were grown by Dr. A. Lopez-Otero, at the University of Linz. We thank the Deutsche Forschungsgemeinschaft for the financial support.

---

*The experiments reported here were performed at the high magnetic field facility of the Max-Planck Institut für Festkörperforschung Grenoble, France.

[1]E. D. Palik and D. L. Mitchell, in *Physics of Solids in Intense Magnetic Fields*, edited by E. D. Haidemenakis (Plenum, New York, 1969), p. 90. The paper describes effects of band population on interband magneto-optical transitions, Faraday rotation, and magnetoplasma phenomena, with special emphasis on PbS.

[2]For a review on PbTe see R. Dalven, in *Solid State Physics*, edited by H. Ehrenreich, F. Seitz, and D. Turnbull (Academic, New York, 1973), Vol. 28, p. 179; and Yu. I. Ravich, B. A. Efimova, and I. A. Smirnov, *Semiconducting Lead Chalcogenides* (Plenum, New

York, 1970).
[3]P. R. Wallace, Can. J. Phys. 43, 2162 (1965). Also in *Physics of Solids in Intense Magnetic Fields*, edited by E. D. Haidemenakis (Plenum, New York, 1969), p. 73; see also S. Perkowitz, Phys. Rev. 182, 828 (1969).
[4]D. L. Mitchell and R. F. Wallis, Phys. Rev. 151, 581 (1966).
[5]A. Lopez-Otero, J. Appl. Phys. 48, 446 (1977); Appl. Phys. Lett. 26, 470 (1976); Thin Solid Films 49, 1 (1978).
[6]H. Burkhard, G. Bauer, P. Grosse, and A. Lopez-Otero, Phys. Status Solidi B 76, 259 (1976).
[7]H. Burkhard, G. Bauer, and A. Lopez-Otero, J. Opt. Soc. Am. 67, 943 (1977).
[8]R. L. Bernick and L. Kleinman, Solid State Commun. 8, 569 (1970).
[9]G. Martinez, M. Schlüter, and M. L. Cohen, Phys. Rev. B 11, 651 (1975); A. Jedrzejcak, D. Guillot, and G. Martinez, *ibid.* 17, 829 (1978).
[10]J. O. Dimmock, in *Proceedings of the International Conference on the Physics of Semimetals and Narrow Gap Semiconductors, Dallas, 1969,* edited by D. L. Carter and R. T. Bate (Pergamon, New York, 1971), p. 319.
[11]R. Grisar, H. Burkhard, G. Bauer, and W. Zawadzki, in *Proceedings of the International Conference on the Physics of Narrow Gap Semiconductors, Warsaw,* edited by J. Rauluszkiewicz (PWN-Polish Scientific, Warsaw, 1978), p. 115.
[12]G. A. Baraff, Phys. Rev. 137, A 842 (1965).
[13]M. S. Adler, C. R. Hewes, and S. D. Senturia, Phys. Rev. B 7, 5186 (1973).
[14]For a review see E. D. Palik and J. K. Furdyna, Rep. Prog. Phys. 33, 1193 (1970), and references cited therein.
[15]D. D. Buss and M. A. Kinch, J. Nonmetals 1, 111 (1973).
[16]J. C. Ramage, F. Kuchar, R. A. Stradling, and A. Lopez-Otero, J. Phys. C 10, 611 (1977); also in Ref. 11, p. 125.
[17]P. R. Wallace, Phys. Status Solidi B 38, 715 (1970).
[18]P. Vogl, in Ref. 11, p. 131; G. Bauer, H. Burkhard, and P. Vogl, Verh. Dtsch. Phys. Ges. VI, 12, 131 (1977).
[19]W. Zawadzki, Adv. Phys. 23, 435 (1974).
[20]S. Tosima, J. J. Quinn, and M. A. Lampert, Phys. Rev. 137, A833 (1965).
[21]G. Bauer, H. Burkhard, W. Jantsch, F. Unterleitner, and A. Lopez-Otero, in *Proceedings of the International Conference on Lattice Dynamics, Paris, 1977,* edited by M. Balkanski (Flammarion, Paris, 1978), p. 669.
[22]H. Kawamura, in Ref. 11, p. 7; P. Grosse, *ibid.*, p. 41.
[23]W. E. Tennant and J. A. Cape, Phys. Rev. B 13, 2540 (1976); W. E. Tennant, Solid State Commun. 20, 613 (1976).
[24]P. M. Amirtharaj, B. L. Bean, and S. Perkowitz, J. Opt. Soc. Am. 67, 939 (1977).
[25]H. Burkhard, G. Bauer, P. Grosse, and A. Lopez-Otero, in *Proceedings of the Thirteenth International Conference on the Physics of Semiconductors*, edited by F. G. Fumi (Marves, Rome, 1976), p. 439; Physica (Utr.) B89, 22 (1977).
[26]G. D. Mahan, in *Polarons in Ionic Crystals and Polar Semiconductors*, edited by J. T. Devreese (North-Holland, Amsterdam, 1972), p. 553.
[27]R. W. Stimets and B. Lax, Phys. Rev. B 1, 4720 (1970).
[28]B. D. McCombe, R. J. Wagner, S. Teitler, and J. J. Quinn, Phys. Rev. Lett. 28, 37 (1972); K. L. Ngai, E. N. Economu, and J. Ruvalds, Phys. Rev. B 6, 2506 (1972).
[29]P. Vogl and P. Kocevar, in *Proceedings of the Fourteenth International Conference on the Physics of Semiconductors, Edinburgh, 1978,* edited by B. L. H. Wilson (Institute of Physics, London, 1979), p. 1317.
[30]C. K. N. Patel and R. E. Slusher, Phys. Rev. 177, 1200 (1969).
[31]R. L. Aggarwal, U. Smith, and B. Lax, in *Proceedings of the Ninth Conference on the Physics of Semiconductors*, edited by M. Ryvkin (Nauka, Leningrad, 1968), p. 337; U. Smith, R. L. Aggarwal, T. P. Tao, and B. Lax, J. Nonmetals 1, 311 (1973).
[32]D. M. Gureev, I. I. Zasavitsky, B. N. Matsonashvili, and A. P. Shotov, in Ref. 11, p. 109, and references cited therein.
[33]G. A. Antcliffe and S. G. Parker, J. Appl. Phys. 44, 4145 (1973).
[34]C. R. Hewes, M. S. Adler, and S. D. Senturia, Phys. Rev. B 7, 5195 (1973).
[35]G. M. T. Foley and D. N. Langenberg, Phys. Rev. B 15, 4830 (1977); 15, 4850 (1977).
[36]H. Kawamura, S. Nishikawa, and S. Nishi, in Ref. 25, p. 310.
[37]H. D. Drew and S. W. McKnight, Bull. Am. Phys. Soc. 22, 472 (1977). These data were taken at H_2O laser frequencies at very low temperatures. According to H. D. Drew (private communication) excitonlike effects might be important. Another interpretation for these comparatively low masses may be that impurity transitions as suggested by Ramage *et al.* (Ref. 16) were taken for cyclotron transitions. However, more work should be devoted to this problem.
[38]G. Burns and E. Burstein, Ferroelectrics 7, 297 (1974); G. Burns, Phys. Rev. B 13, 215 (1976).
[39]H. Schaber, R. E. Doezema, J. F. Koch, and A. Lopez-Otero, Solid State Commun. 26, 7 (1978).